
Variance Reduction in Deep Learning: More Momentum is All You Need.

Lionel Tondji^{1,2} Sergii Kashubin³ Moustapha Cisse³

Abstract

Variance reduction (VR) techniques have contributed significantly to accelerating learning with massive datasets in the smooth and strongly convex setting (Schmidt et al., 2017; Johnson & Zhang, 2013; Roux et al., 2012). However, such techniques have not yet met the same success in the realm of large-scale deep learning due to various factors such as the use of data augmentation or regularization methods like dropout (Defazio & Bottou, 2019). This challenge has recently motivated the design of novel variance reduction techniques tailored explicitly for deep learning (Arnold et al., 2019; Ma & Yarats, 2018). This work is an additional step in this direction. In particular, we exploit the ubiquitous clustering structure of rich datasets used in deep learning to design a family of scalable variance reduced optimization procedures by combining existing optimizers (e.g., SGD+Momentum, Quasi Hyperbolic Momentum, Implicit Gradient Transport) with a multi-momentum strategy (Yuan et al., 2019). Our proposal leads to faster convergence than vanilla methods on standard benchmark datasets (e.g., CIFAR and ImageNet). It is robust to label noise and amenable to distributed optimization. We provide a parallel implementation in JAX.

1. Introduction

Given a data generating distribution \mathbb{P} , a parameterized function f_θ (e.g. a deep network) and a loss function $\ell(\cdot)$, we consider the traditional risk minimization problem representative of most settings in ML (Shalev-Shwartz & Ben-David, 2014):

$$\theta^* = \arg \min_{\theta} \mathbb{E}_{(x \sim \mathbb{P})} \ell(f_\theta(x)) \quad (1)$$

The celebrated optimization algorithm for solving this problem in large-scale machine learning is Stochastic Gradient

Descent (SGD) (Robbins, 2007; Bottou et al., 2018). In favorable cases (e.g., smooth and strongly convex functions), SGD converges to a good solution by iteratively applying the following first-order update rule: $\theta_{t+1} \leftarrow \theta_t - \mu_t g(x_t, \theta_t)$ where x_t is an instance drawn from \mathbb{P} , μ_t is the learning rate and $g(x_t, \theta_t)$ is the (approximate) gradient. SGD enjoys several desirable properties. Indeed, It is fast: when one has access to the actual gradient, its convergence rate is $O(e^{-\nu t})$ for some $\nu > 0$. Also, it is memory efficient, robust, and amenable to distributed optimization (Bottou et al., 2018; Nemirovski et al., 2009; Dean et al., 2012). However, we generally do not know the data-generating distribution \mathbb{P} ; consequently, we do not have access to the actual gradient. Instead, we resort to empirical risk minimization and rely on a stochastic approximation of the gradient for a given x_t and θ_t . Unfortunately, the gradient noise due to using the approximate instead of the exact gradient slows down the convergence speed (which becomes $O(1/t)$ instead of $O(e^{-\nu t})$) (Bottou et al., 2018). It also makes the algorithm harder to tune. Variance Reduction (VR) techniques allow us to mitigate the impact of using noisy gradients in stochastic optimization (Roux et al., 2012; Defazio et al., 2014; Johnson & Zhang, 2013; Mairal, 2013).

Variance reduction methods have been successfully applied to convex learning problems (Roux et al., 2012; Defazio et al., 2014; Shalev-Shwartz & Zhang, 2013; Johnson & Zhang, 2013). However, this success does not readily translate to large-scale non-convex settings such as deep learning due to colossal memory requirements (Roux et al., 2012; Defazio et al., 2014; Shalev-Shwartz & Zhang, 2013) and the use of normalization and data augmentation procedures (Defazio & Bottou, 2019). This has motivated the design of novel VR strategies that are better suited for deep learning (Cutkosky & Orabona, 2019; Arnold et al., 2019; Ma & Yarats, 2018). In the next section, we present in more detail *Implicit Gradient Transport* (Arnold et al., 2019) and *Quasi Hyperbolic Momentum* (Ma & Yarats, 2018), two instances of successful application of VR to deep learning.

Large scale datasets used in deep learning problems come with a rich clustering structure (Deng et al., 2009). For example, the data can result from the aggregation of several datasets collected by different individuals or organizations (e.g., this is typical in the federated learning setting (Li et al., 2019)). When there is an underlying clustering structure

¹Institute of Analysis and Algebra, TU Braunschweig ²This work was done during the AI Residency at Google Brain ³Google Research, Brain Team. Correspondence to: Lionel Tondji <l.ngoupeyou-tondji@tu-braunschweig.de>

in the data, the variance due to gradient noise decomposes into an in-cluster variance and a between-cluster variance. Yuan et al. (2019) exploit this insight to reduce the between cluster variance in the convex setting by considering every data point as a separate cluster. Unfortunately, such an approach requires storing as many models as data points and therefore has prohibitive memory requirements. Also, it does not consider the use of mini-batches during training. Consequently, it is not directly applicable to deep learning.

In this work, we make the following contributions:

- We leverage the idea of *using multiple momentum terms* and introduce a family of variance reduced optimizers for deep learning. These new approaches (termed Discover¹) improve upon widely used methods such as SGD with Momentum, IGT, and QHM. They are theoretically well-motivated and can exploit the clustering structures ubiquitous in deep learning.
- Using simple clustering structures, we empirically validate that Discover optimizers lead to faster convergence and sometimes (significantly) improved generalization on standard benchmark datasets. We provide parallel implementations of our algorithms in JAX².

In the next section, we provide a brief overview of variance reduction methods with an emphasis on Implicit Gradient Transport (Arnold et al., 2019) and Quasi Hyperbolic Momentum (Ma & Yarats, 2018), two VR optimizers specifically designed for deep learning. We then discuss (section 3) the clustering structure present in most deep learning problems and how we can leverage it to design scalable variance reduction strategies. The experiments section demonstrates our proposals’ effectiveness and provides several insights regarding their behavior.

2. Variance Reduction in Deep Learning

We consider Variance Reduction (VR) in the realm of large-scale deep learning (Goodfellow et al., 2016), i.e. when we are in the presence of significant amounts of (streaming) data, and the parameterized function f_θ is a massive deep neural network. Most existing approaches do not naturally scale to this setting. Indeed, dual methods for VR, such as SDCA (Shalev-Shwartz & Zhang, 2013), have prohibitive memory requirements due to the necessity of storing large dual iterates. Primal methods akin to SAGA (Roux et al., 2012) are also memory inefficient because they need to store past gradients. Other approaches like SARAH (Nguyen et al., 2017) are computationally demanding; they entail a full snapshot gradient evaluation at each step and two mini-batch evaluations. While some recent approaches, such as

stochastic MISO (Bietti & Mairal, 2017), can handle infinite data in theory. However, their memory requirement scales linearly with the number of examples. In addition to these limitations, Defazio & Bottou (Defazio & Bottou, 2019) have shown that several other factors such as data augmentation (Krizhevsky et al., 2012), batch normalization (Ioffe & Szegedy, 2015), or dropout (Srivastava et al., 2014b) impede the success of variance reduction methods in deep learning. Despite these negative results, some recent approaches such as Quasi Hyperbolic Momentum (Ma & Yarats, 2018) and Implicit Gradient Transport with tail averaging (IGT) (Arnold et al., 2019) have shown promising results in variance reduction in the context of large scale deep learning. In the sequel, we present them in more detail. We first present the Momentum or Heavy Ball method since the above approaches and our proposal rely on it.

The Momentum or Heavy Ball (Polyak, 1964; Sutskever et al., 2013) method uses the following update rule:

$$\begin{aligned} v_t &= \beta v_{t-1} + (1 - \beta) \cdot g(\theta_t, x_t) \\ \theta_{t+1} &= \theta_t - \mu v_t \end{aligned}$$

where v_t is called the momentum buffer and β_t balances the buffer and the approximate gradient compute at iteration t . SGD with Momentum is widely used in deep learning due to its simplicity and its robustness to variations of hyperparameters (Sutskever et al., 2013; Zhang & Mitliagkas, 2017). It is an effective way of alleviating slow convergence due to curvature (Goh, 2017) and has been recently shown also perform variance reduction (Roux et al., 2018).

The Quasi Hyperbolic Momentum (QHM) (Ma & Yarats, 2018) method uses the following update rule:

$$\begin{aligned} v_t &= \beta v_{t-1} + (1 - \beta) \cdot g(\theta_t, x_t) \\ \theta_{t+1} &= \theta_t - \mu \cdot [\nu v_t + (1 - \nu)g(\theta_t, x_t)] \end{aligned}$$

QHM extends Momentum by using in the update a combination of the approximate gradient and the momentum buffer. When $\nu = 1$ (resp. $\nu = 0$), it reduces to Momentum (resp. SGD). QHM inherits the efficiency of Momentum and also performs VR. In addition, it alleviates the potential staleness of the momentum buffer (when choosing $\nu < 1$).

The Implicit Gradient Transport (IGT) (Arnold et al., 2019) method uses the following update rule:

$$\begin{aligned} \gamma_t &= t/(t + 1) \\ v_t &= \gamma_t \cdot v_{t-1} + (1 - \gamma_t) \cdot g\left(\theta_t + \frac{\gamma_t}{1 - \gamma_t}(\theta_t - \theta_{t-1}), x_t\right) \\ w_t &= \beta \cdot w_{t-1} - \mu \cdot v_t \\ \theta_{t+1} &= \theta_t + w_t \end{aligned}$$

IGT effectively achieves variance reduction by combining several strategies maintaining a buffer of past gradients (us-

¹Deep SCAlable Online Variance Reduction

²<https://github.com/google/jax>

ing iterative tail averaging) and transporting them to equivalent gradients at the current point. The resulting update rule can also be combined with Momentum as shown above.

3. Exploiting Clusters in Variance Reduction

The Ubiquitous Clustering Structure Large-scale machine learning datasets come with a rich clustering structure that arises in different ways depending on the setting. For example, when training deep neural networks, we combine various data augmentation strategies, resulting in a mixture with clusters defined by the transformations (Zhang et al., 2017; Yun et al., 2019b; Krizhevsky et al., 2012). In multi-class classification problems, one can consider each class as a separate cluster. Therefore, the overall dataset becomes a mixture defined by the classes. In all these cases, the data is not independent and identically distributed across clusters. Indeed, different data augmentation strategies lead to different training data distributions. To make the clustering structure apparent, we can rewrite the minimization problem in equation 1 as a combination of risks on the different clusters. To this end, we denote \mathbb{P}_n the data distribution corresponding to the n -th cluster and p_n the probability with which we sample from that cluster, with $\sum_{n=1}^N p_n = 1$. We also denote x_t^n the realization of the data point x_t belonging to the cluster n for clarity. The risk minimization problem 1 becomes:

$$\theta^* = \arg \min_{\theta} \sum_{n=1}^N p_n \mathbb{E}_{(x \sim \mathbb{P}_n)} \ell(f_{\theta}(x)) \quad (2)$$

While one can pool all the data to apply traditional empirical risk minimization 1, this would ignore valuable *prior clustering information*. In the next section, we show how, when solving the equivalent problem 2, we can leverage the clustering information to speed the learning procedure by reducing the variance due to gradient noise. We start with stochastic gradient descent and present a decomposition of such variance, which considers the clustering structure.

Gradient noise for SGD with clusters Here, we re-derive the variance of the gradient noise for SGD in presence of clustered data (Sayed, 2014b; Yuan et al., 2019). To this end, we introduce the filtration $F_t = \{\theta_{i < t+1}\}$ and denote $g_n(\theta) = \mathbb{E}_{(x^n \sim \mathbb{P}_n)} g(\theta, x^n)$ for convenience. We assume the loss $\ell(f(x^n))$ is δ -Lipschitz with respect to θ and the clustered risk $\ell_n(\theta) = \mathbb{E}_{(x \sim \mathbb{P}_n)} \ell(f_{\theta}(x^n))$ is ν -strongly convex, that is for any θ_1, θ_2 it holds:

$$(g_n(\theta_1) - g_n(\theta_2))^T (\theta_1 - \theta_2) \geq \nu \|\theta_1 - \theta_2\|^2$$

For a given example x_t^n , the update rule for stochastic gradient descent is $\theta_{t+1} \leftarrow \theta_t - \mu_t g(x_t^n, \theta_t)$. The gradient noise resulting from this update depends both on the probability distribution on the clusters and the data distribution \mathbb{P}_n for

the considered cluster. For a given example, the gradient noise writes: $s_{t+1}(\theta_t) = g(x_t^n, \theta_t) - g(\theta_t)$ and the gradient noise *within* the cluster n is: $s_{t+1}^n(\theta_t) = g(x_t^n, \theta_t) - g_n(\theta_t)$. The following result bounds the first and second moment of the within-cluster variance of the gradient noise for SGD.

Lemma 1 *The first and second order moments of the gradient noise $s_{t+1}(\theta_t)$ satisfy: $\mathbb{E}(s_{t+1}(\theta_t)|F_t) = 0$ and $\mathbb{E}(\|s_{t+1}(\theta_t)\|^2|F_t) \leq \beta^2 \|\tilde{\theta}_t\|^2 + \sigma^2$ where $\beta^2 = 2\delta^2$, $\tilde{\theta}_t = \theta_t - \theta^*$ and $\sigma^2 = 2\mathbb{E}(\|g(x_t^n, \theta^*)\|^2|F_t)$.*

We can now decompose the variance of the gradient noise into a sum of *within-cluster* and *between-cluster* variance.

Lemma 2 *Assuming the gradient is unbiased and the variance of the gradient noise within the cluster n is bounded as in shown in lemma 1, the following inequality holds:*

$$\mathbb{E}(\|s_{t+1}(\theta^*)\|^2|F_t) \leq \underbrace{\sum_{n=1}^N p_n \sigma_n^2}_{\text{in-cluster variance}} + \underbrace{\sum_{n=1}^N p_n \|g_n(\theta^*)\|^2}_{\text{between-cluster variance}} \quad (3)$$

Lemma 2 captures the structure of the problem. The LHS represents the variance of the gradient noise. The first term of the RHS is the within-cluster variance σ_{in}^2 , and the second term is the between-cluster variance σ_{bet}^2 . In the limit, the mean square deviation of the steady-state depends on the in-cluster and between-cluster variances as follows $\limsup_{t \rightarrow \infty} \|\theta_t - \theta^*\| = O(\mu(\sigma_{in}^2 + \sigma_{bet}^2))$. Therefore when the clustering structure is known and $\sigma_{in}^2 \ll \sigma_{in}^2 + \sigma_{bet}^2$, which is our working assumption, we can significantly reduce the overall variance by reducing the between-cluster variance. In the next section, we present an update rule exploiting this fact and generalizing the approach presented in (Yuan et al., 2019) to the minibatch setting³. We also prove its gradient noise properties and convergence⁴

4. Discover Algorithms

To re-iterate, we assume we know the clustering structure and the probability p_n of observing data from a given cluster n such that $\sum_n p_n = 1$. As we will show in the experiments, this is a realistic assumption, and straightforward design choices such as using labels or data augmentation strategies as clusters lead to improved results. We do not have access to the data distribution given a cluster n . We consider a

³It is worth noting that Yuan et al. (2019) have assumed the results in lemma 1 and state lemma 2 without proof. We provide full proofs in the appendix.

⁴The proof assumes a smooth and strongly convex setting. Though we consider in the experiments non-convex problems, this assumption may be valid locally in a basin of attraction of the loss landscape of a deep neural network

learning setting where at each round t , we observe a batch of examples $\mathcal{B}_t = \{x_t^n\}$ coming from the different groups and sampled according to the mixture distribution induced by the clustering structure. We propose to achieve between cluster variance reduction in minibatch stochastic gradient descent by recursively applying the following update rule:

$$\theta_{t+1} = \theta_t - \frac{\mu}{|\mathcal{B}_t|} \cdot \sum_{x_t^n \in \mathcal{B}_t} \left(g(x_t^n, \theta_t) - g_t^{(n)} + \sum_{k=1}^N p_k g_t^{(k)} \right) \quad (4)$$

The update rule stems from the traditional use of control variates for variance reduction (Fishman, 1996) with the additional trick to use one control variate for each cluster given that the clustering structure is known. In Equation (4), each $g_t^{(n)}$ is an approximation of the actual cluster gradient $g_n(\theta_t)$ to which the example x_t^n belongs, and $\bar{g}_t = \sum_{k=1}^N p_k g_t^{(k)}$ is the average cluster gradient. The gradient noise resulting from the update rule 4 depends both on the probability distribution on the clusters and the data distribution \mathbb{P}_n of each considered cluster. It can be written as follows:

$$u_{t+1}(\theta_t) = \frac{1}{|\mathcal{B}_t|} \cdot \sum_{x_t^n \in \mathcal{B}_t} \left(g(x_t^n, \theta_t) - g_t^{(n)} + \bar{g}_t \right) - g(\theta_t)$$

In the sequel, we show how a recursive application of the above update rule ultimately leads to reduced between-cluster variance of the gradient noise $u_{t+1}(\theta_t)$. Before, we first state a lemma exposing the properties of the gradient noise $u_{t+1}(\theta_t)$. Similarly to Lemma 2, this results highlights how the variance of the gradient noise decomposes into an in-cluster and a between-cluster variance. We provide a proof of the lemma in the appendix Section 9.1.

Lemma 3 (*gradient noise properties*) *Under the same assumptions as in Section 3, for a batch of size $|\mathcal{B}_t|$ the gradient is unbiased $E[u_{t+1}(\theta_t)|F_t] = 0$. Denoting $\theta_t := \theta^* - \theta_t$, $C_1 = 4\delta^2$ and $\sigma_n^2 = 2 \cdot \mathbb{E}(\|g(x_t^n, \theta^*)\|^2)$ the variance of the gradient noise is bounded as:*

$$\mathbb{E} \left(\|u_{t+1}(\theta_t)\|^2 | F_t \right) \leq \frac{1}{|\mathcal{B}_t|} \cdot C_1 \|\tilde{\theta}_t\|^2 + \underbrace{\frac{1}{|\mathcal{B}_t|} \cdot \sum_{n=1}^N p_n \sigma_n^2}_{\text{in-cluster variance}} + \underbrace{\frac{2}{|\mathcal{B}_t|} \cdot \sum_n p_n \|g_t^{(n)} - g_n(\theta^*)\|^2}_{\text{between-cluster variance}} \quad (5)$$

Remark The second and the last term of the right-hand side of this bound are respectively the within-cluster and the between-cluster variance. If the approximate cluster gradient converges to the actual one $g_t^{(n)} \rightarrow g_n(\theta^*)$ as $t \rightarrow \infty$, the between-cluster variance vanishes. It is worth noting

Algorithm 1 Discover

Initialization: $\bar{g}_0 = 0, \alpha \in (0, p_{\min}), g_0^{(n)} = 0, \alpha_n = \alpha/p_n$
for $t = 0, \dots, T - 1$ **do**

 Get the cluster indexes \mathcal{C} in the current batch \mathcal{B}_t and
 update $\theta_{t+1}, \{g_{t+1}^{(n)}\}_{n=1}^N$ and \bar{g}_{t+1} :

$$\theta_{t+1} = \theta_t - \frac{\mu}{|\mathcal{B}_t|} \cdot \sum_{x_t^n \in \mathcal{B}_t} \left(g(x_t^n, \theta_t) - g_t^{(n)} + \bar{g}_t \right)$$

for $n \in \mathcal{C}$ **do** ▷ in parallel

$$\mathcal{B}_t^n = \{x_t^k \in \mathcal{B}_t \mid k = n\}$$

$$g_{t+1}^{(n)} = (1 - \alpha_n)g_t^{(n)} + \frac{\alpha_n}{|\mathcal{B}_t^n|} \sum_{x_t^n \in \mathcal{B}_t^n} g(x_t^n, \theta_t)$$

end for

$$g_{t+1}^{(n)} = g_t^{(n)} \text{ for each } n \notin \mathcal{C}$$

$$\bar{g}_{t+1} = \bar{g}_t - \frac{\alpha}{|\mathcal{B}_t|} \sum_{x_t^n \in \mathcal{B}_t} \left(g_t^{(n)} - g(x_t^n, \theta_t) \right)$$

end for

return θ_T

that when we use the same approximate gradient buffer g^M for all the clusters, the update rule 4 reduces to that of SGD with Momentum (Polyak, 1964; Goh, 2017). Consequently, the between cluster variance term in the above bound becomes $(2/|\mathcal{B}_t|) \cdot \|g_t^M - g_n(\theta^*)\|^2$ and may vanish as $t \rightarrow \infty$. Therefore, Momentum also can perform between-cluster variance reduction and can be seen as a special case of the method proposed here, albeit operating at a coarser level (maintaining one general approximate cluster gradient buffer instead of one for each cluster). Momentum has been mainly considered as a method for fighting curvature (Goh, 2017). Recent work has shown its variance reduction capabilities in specific cases (Roux et al., 2018). We show in our experiments that Momentum indeed performs between-cluster variance reduction. We now show that recursive applications of the update rule 4 indeed leads to vanishing between-cluster variance. The full proof of Theorem 1 is provided in the appendix Section 9.3.

Theorem 1 *Under the same assumptions as in Section 3, we denote $|\mathcal{B}_t|$ as the batch size and $\sigma_{in}^2 = \sum_{n=1}^N p_n \sigma_n^2$ as the in-cluster variance with $\sigma_n^2 = 2 \cdot \mathbb{E}(\|g(x_t^n, \theta^*)\|^2)$, $p_{\min} = \min\{p_1, \dots, p_N\}$. For any step size satisfying*

$$\mu \leq \min \left\{ \frac{\nu |\mathcal{B}_t|}{3\delta^2(|\mathcal{B}_t|+5)}, \frac{\alpha}{6\nu} \right\} \text{ where } \alpha \in (0, p_{\min}) \text{ and}$$

$\gamma = \frac{3\mu^2}{\alpha|\mathcal{B}_t|}$, the iterate θ_t from Discover 1 converge in expectation to the solution θ^* with the contraction factor $q = 1 - \mu\nu < 1$ with $G_0 = \sum_{n=1}^N p_n \|g_n(\theta^*)\|^2$. it holds:

$$\mathbb{E}(\|\theta_t - \theta^*\|^2) \leq q^t \left(\mathbb{E}(\|\tilde{\theta}_0\|^2) + \gamma G_0 \right) + \frac{4\mu}{\nu|\mathcal{B}_{t-1}|} \sigma_{in}^2 \quad (6)$$

$$\limsup_{t \rightarrow +\infty} \mathbb{E}(\|\theta_{t+1} - \theta^*\|^2) = O(\mu \cdot \sigma_{in}^2 / |\mathcal{B}_t|) \quad (7)$$

Theorem 1 shows that when the step size is small, Discover 1 eliminates the between-cluster variance in the limit, hence

reducing the overall variance of the gradient noise to the in-cluster variance. Therefore, when the latter is significantly smaller than the between-cluster variance, Discover can be an effective variance reduction strategy. We show in the experiments section that when the clustering structure to exploit is carefully chosen, Discover leads to faster convergence and sometimes results in improved generalization thanks to the cluster information. We now show how to leverage the idea of using multiple momentum terms based on a given clustering to improve Implicit Gradient Transport (Arnold et al., 2019) and Quasi Hyperbolic Momentum (Ma & Yarats, 2018) (both relying on a single momentum in their vanilla version). The update rules for such extensions (respectively called Discover-IGT and Discover-QHM) follow. Our experiments will demonstrate the effectiveness of these methods.

Discover-IGT (D-IGT) update rule :

$$\begin{aligned}\gamma_t &= t/(t+1) \\ v_t &= \gamma_t \cdot v_{t-1} + (1 - \gamma_t) \cdot g\left(\theta_t + \frac{\gamma_t}{1 - \gamma_t}(\theta_t - \theta_{t-1}), x_t\right) \\ g_{t+1}^{(n)} &= \begin{cases} (1 - \alpha_n)g_t^{(n)} + \alpha_n v_t & \text{if } n \in \mathcal{C}, \\ g_t^{(n)} & \text{otherwise} \end{cases} \\ \theta_{t+1} &= \theta_t - \frac{\mu}{|\mathcal{B}_t|} \cdot \sum_{x_t^n \in \mathcal{B}_t} \left(v_t - g_t^{(n)} + \bar{g}_t \right)\end{aligned}$$

The Discover-QHM (D-QHM) method uses the following update rule:

$$\begin{aligned}g_{t+1}^{(n)} &= \begin{cases} (1 - \alpha_n)g_t^{(n)} + \frac{\alpha_n}{|\mathcal{B}_t^n|} \sum_{x_t^n \in \mathcal{B}_t^n} g(x_t^n, \theta_t) & \text{if } n \in \mathcal{C}, \\ g_t^{(n)} & \text{otherwise} \end{cases} \\ g_{t+2}^{(n)} &= \nu g_{t+1}^{(n)} + (1 - \nu) \cdot \frac{1}{|\mathcal{B}_t^n|} \sum_{x_t^n \in \mathcal{B}_t^n} g(x_t^n, \theta_t) \\ \theta_{t+1} &= \theta_t - \frac{\mu}{|\mathcal{B}_t|} \cdot \sum_{x_t^n \in \mathcal{B}_t} \left(g(x_t^n, \theta_t) - g_{t+1}^{(n)} + \bar{g}_{t+1} \right)\end{aligned}$$

where $\mathcal{B}_t^n = \{x_t^k \in \mathcal{B}_t \mid k = n\}$ is the batch at iteration t , \mathcal{C} is the cluster indexes present in the batch \mathcal{B}_t , and $g_t^{(n)}$ are updated in parallel for $n \in \mathcal{C}$. Discover-IGT combines gradient transport and the multi-momentum strategy. D-QHM extends QHM and Discover by using in the update a combination of the approximate gradient and the momentum buffer, together with a multi-momentum approach similar to Discover. When $\nu = 1$, and $N = 1$ it reduces to Momentum. When $N = 1$, it reduces to QHM. When $\nu = 1$, it reduces to Discover. Choosing $\nu < 1$ alleviates the potential staleness of the buffer.

5. Experiments

We validate that the Discover algorithms coupled with a careful clustering structure lead to faster convergence compared to their vanilla counterparts (SGD+Momentum, IGT, and QHM⁵). We provide additional insights and show that the runtime is comparable to competing methods thanks to a careful parallel implementation.

We implement all the methods used in our experiments using JAX (Bradbury et al., 2018), and FLAX (Flax Developers, 2020) and perform our experiments on Google Cloud TPU (Jouppi et al., 2017) devices. We compare Discover with widely used minibatch SGD with Momentum, and Adam (Kingma & Ba, 2014), as well as with the more recently introduced IGT and QHM on ImageNet (Deng et al., 2009) and CIFAR-10 (Krizhevsky et al., 2009) datasets. Discover is amenable to parallelization. For example, at each round, we can update the cluster gradients in parallel, as shown in Algorithm 1. Our implementation exploits this feature and groups clusters by cores to enable parallel updates. That is, examples of each core belong to the same cluster. In this section we treat α_n as an independent hyperparameter instead of using an exact equation $\alpha_n = \alpha/p_n$ to simplify the parallel implementation. We provide more details about the practical implementation in appendix Section 7.1. We confirm that using the same strategy does not make a practical difference for all the other optimizers we consider. For each optimizer, we select the hyperparameters either as suggested by its authors or by running a sweep to obtain the highest accuracy at the end of training across five random seeds. The details of the training setup, HP search, and the best values found for each optimizer are given in appendix Section 7.

ImageNet: Data augmentation methods as clusters

We first consider an image classification and train a ResNet-v1-50 (He et al., 2016) model on the ImageNet (Deng et al., 2009; Russakovsky et al., 2015) dataset for 31200 steps (90 epochs). We use cosine learning rate schedule with minibatches of a batch size of 4096, weight decay regularization of 0.001, group normalization (Wu & He, 2018), and weight standardization (Qiao et al., 2019). We use a standard pre-processing pipeline consisting of cropping (Szegedy et al., 2015) with size 224x224, pixel value scaling, and a random horizontal flipping.

We train our Resnet-50 using three data augmentation methods: random flipping, Mixup (Zhang et al., 2017), and CutMix (Yun et al., 2019a). For each image, we apply all transformations separately, producing three differently augmented examples (as shown in Figure 5). *Consequently, each of the augmentation methods induces a differ-*

⁵we restrict QHM to $\nu \neq 0$ and $\nu \neq 1$ so it is not reduced to SGD or SGD+Momentum

ent cluster and the probability of each is $1/3$. We compare the multi-momentum strategies (Discover, Discover-IGT, and Discover-QHM), exploiting this clustering information, with their vanilla counterparts (SGD with Momentum, IGT, and QHM). For the sake of completeness, we also add Adam to the comparison as a baseline. Figure 1 shows the results for the different methods. Using all these data augmentation methods can make the learning problem more difficult because the resulting cluster data distributions can differ significantly. In this setting, we observe that Discover variants initially converge faster than their corresponding vanilla optimizers. Discover, and Discover-IGT reach similar final performance to SGD with Momentum and IGT, respectively, while Discover-QHM outperforms the vanilla QHM.

CIFAR: Classes as clusters. Next, we consider the CIFAR-10 (Krizhevsky et al., 2009) classification and use the classes as the clusters, therefore having ten different clusters. We train a WideResNet26-10 (Zagoruyko & Komodakis, 2016) on CIFAR-10 for 400 epochs using cosine learning rate schedule, batch size of 256, group normalization, L2-regularization of 5×10^{-4} and dropout rate of 0.3. The preprocessing consists of 4-pixel zero-padding, a random crop of size 32x32, scaling the pixels to $[0, 1]$ range and random horizontal flip.

Figure 2 shows the results for the different optimizers. CIFAR-10 is an easy task and all the methods eventually converge to high accuracy. IGT converges faster than Discover-IGT and reaches higher final accuracy (95.3% vs 94.2%). Discover (resp. Discover-QHM) converge similarly to SGD with Momentum (resp. QHM). These single momentum strategies also reach a similar (for QHM, 95.1% vs 95.4%) or higher (for Momentum, 95.3% vs 94.2%) final performance. To highlight the importance of carefully choosing the clustering structure, we also performed an experiment on CIFAR-10 where we assigned each point to 1 of 10 clusters *uniformly at random* and train the model using discover and such clustering. The resulting test accuracy is 91.09% down from 94.2% when using classes as clusters. Therefore it is essential to use a good clustering structure.

Learning with noisy labels We now consider the more challenging ImageNet and CIFAR-10 classification task *in the presence of label noise*: At each round, the label of the considered example is flipped with probability p (the noise level) and assigned to a different class selected uniformly at random among the other classes. In this setting, the variance of the gradient noise is increased due to the presence of label noise (see Appendix Section 8). We compare Discover, Discover-QHM, and Discover-IGT with their vanilla counterparts (SGD with Momentum, QHM, IGT) and Adam. We use Data augmentation methods as clusters for ImageNet and classes as clusters for CIFAR-10. We use the same

Table 1. Training performance (in steps/second) with different optimizers. On ImageNet a single number is reported, while on CIFAR - Mean and std deviation across 5 runs.

Optimizer	ImageNet, 64 TPUv3	CIFAR-10 ($\mu \pm \sigma$), 4 TPUv2
SGD	—	14.3 ± 3.8
Adam	8.2	9.8 ± 0.4
Momentum	8.7	10.4 ± 0.7
IGT	7.8	9.3 ± 0.6
QHM	8.6	12.5 ± 2.7
Discover	7.4	6.3 ± 0.3
Discover-QHM	7.6	5.8 ± 0.02
Discover-IGT	7.3	5.6 ± 0.02

setting as in the previous ImageNet and CIFAR-10 experiments. Still, We perform a hyperparameter (HP) search de novo to determine the best learning for each method in the presence of noisy labels. The details of the HP search, and the best values found for each optimizer are given in appendix Section 7.

When the label noise is low ($p = 0.2$), all the methods achieve high accuracy on the non-corrupted training examples and the test examples with only a slight deterioration compared to a clean setting $p = 0$ (exact results are given in appendix Section 7.5). Figure 3 and Figure 4 show the results of this experiment in the high noise level setting ($p = 0.8$) on ImageNet and CIFAR-10, respectively. On CIFAR-10, the multi-momentum optimizers’ loss curves are almost superimposed with the curves of SGD with Momentum, QHM, and IGT. However, the former generalize significantly better at each time step and reach higher final performance than all their single momentum counterparts. It is worth noting that Discover outperforms all the multi-momentum optimizers by a large margin on the validation accuracy, achieving 85.9%. The superiority of multi-momentum optimizers over the single momentum ones translates to ImageNet, suggesting that our Discover algorithms find better local optima even in challenging settings. The other interesting finding is that while Adam converges faster in training loss, it generalizes poorly.

Impact of clustering structure. We also performed an experiment on CIFAR-10 where we compare three clustering structures: (1) Classes as clusters: This is the setting we have considered so far for CIFAR-10. (2) Transformations as clusters. (3) Random clusters: assigning each point to 1 of 10 clusters *uniformly at random*. In each case, we train the model using Discover and the chosen clustering. When the clusters are selected uniformly at random, the resulting test accuracy is 91.09%. When we use transformation as clusters instead, the test accuracy improves to 93.6%. The best accuracy with Discover on CIFAR-10 (94.2%) is achieved when using classes as clusters. However, using this

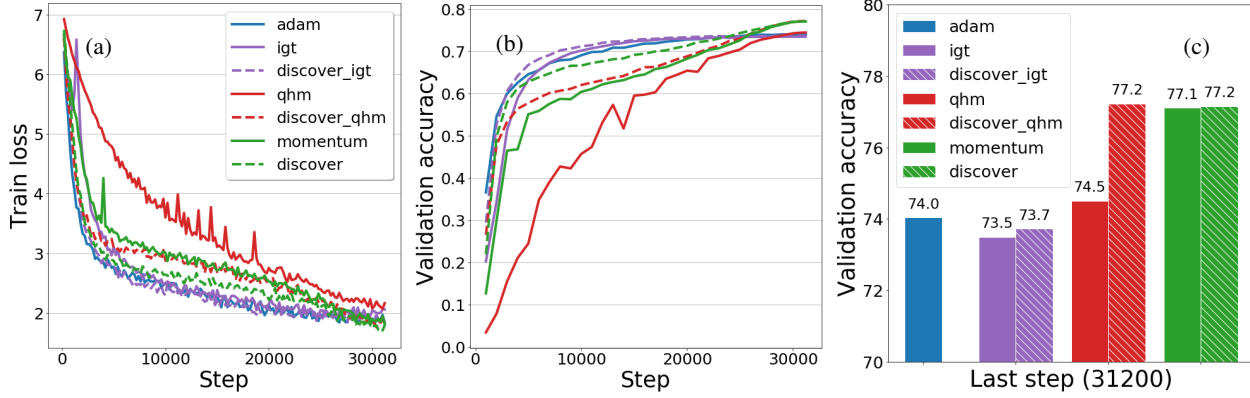


Figure 1. Results of training ResNet-v1-50 model on ImageNet dataset: train loss (a), validation accuracy (b) and validation accuracy on the last step in % (c). Discover consistently stays on par with vanilla optimizers (IGT, Momentum) or outperforms them (QHM) in the end of the training while always converging faster in the beginning.

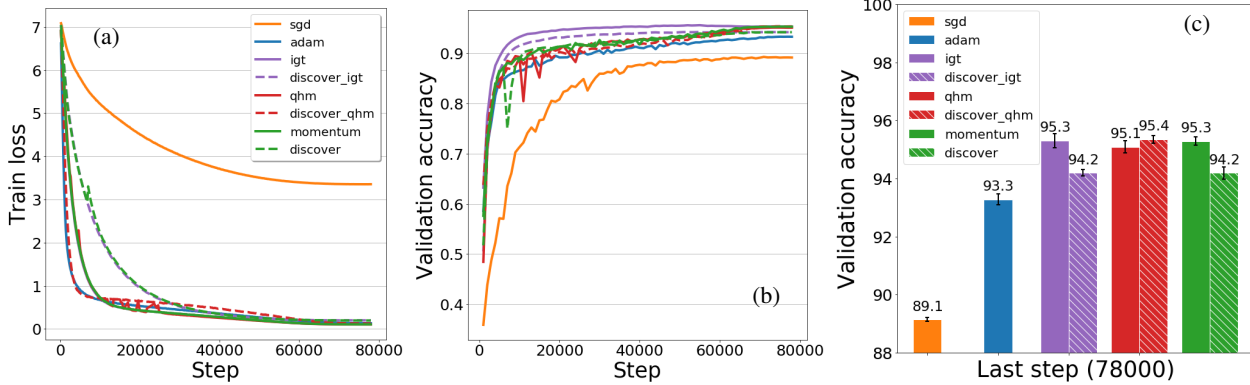


Figure 2. Results of training WideResNet26-10 model on CIFAR-10 dataset (classes as clusters): train loss (a), validation accuracy (b) and validation accuracy on the last step in % (c). For each step a mean value across 5 random seeds is plotted, black whiskers in (c) indicate standard deviation. Discover variants for IGT and Momentum are slightly worse than vanilla optimizers, while being on par for QHM.

clustering structure comes at the cost of a higher memory.

Between-Cluster Variance Reduction In this experiment, we assess the between-cluster variance reduction capabilities of Discover compared to SGD and SGD with Momentum on CIFAR-10 (with classes as clusters) both in the clean ($p = 0$) and noisy ($p = 0.8$) settings. We measure at each step of the optimization an approximation of the between-cluster variance obtained by substituting $g_n(\theta_{t+1})$ to $g_n(\theta^*)$ in the between-cluster variance formula. For SGD we use Equation (3). For Discover and SGD with Momentum – Equation (5). However, for SGD with Momentum, one global gradient buffer is used for all the clusters. Equation (5) shows that in both the clean and the noisy setting, Discover reduces the between-cluster variance faster. The figure also highlights the between-cluster variance reduction capabilities of SGD with Momentum, which, though not as fast as Discover, also leads to quickly vanishing variance. This explains the good performance of Momentum in our

previous experiments.

6. Conclusion and Perspectives

We introduced a set of scalable VR algorithms exploiting the ubiquitous clustering structure in the data and relying on a multi-momentum strategy. We demonstrated that simple choices of clustering structure (e.g., transformations) can lead to improved results. Our framework gives the designer significant flexibility allowing them to leverage prior information to select good clustering structure. The experiments demonstrated that the proposed strategy often leads to faster convergence and sometimes to improved generalization, especially in challenging settings (e.g., label noise).

Table 1 shows there are only minor differences between the multi-momentum strategies and their vanilla counterparts thanks to our efficient implementation that exploits the parallel structure of the algorithms.

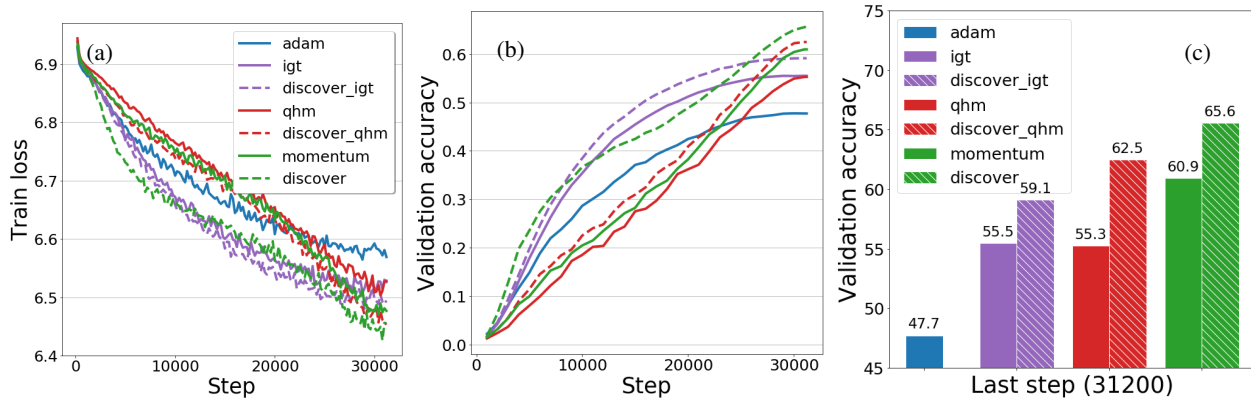


Figure 3. Results of training ResNet-v1-50 model on ImageNet dataset in a high noise setting $p = 0.8$: train loss (a), validation accuracy (b) and validation accuracy on the last step in % (c). Discover variants outperforms all vanilla optimizers by a large margin.

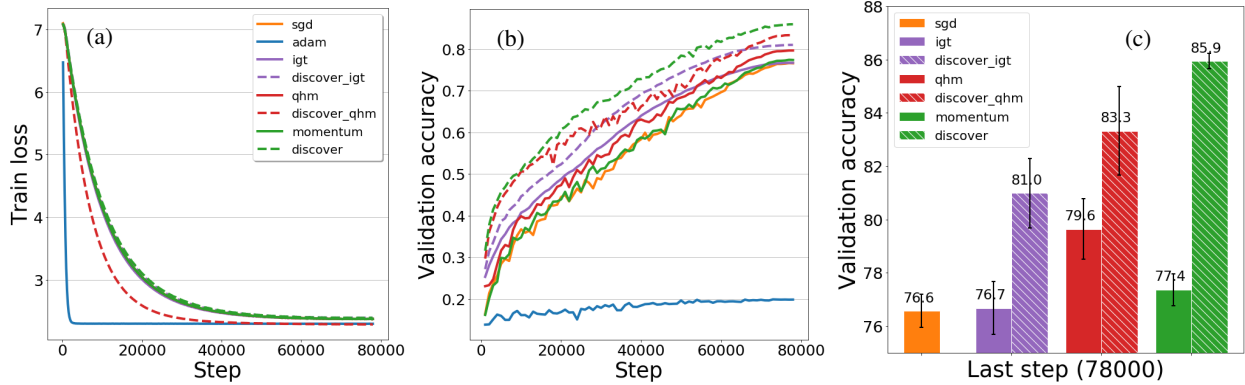


Figure 4. Results of training WideResNet26-10 model on CIFAR-10 dataset (classes as clusters) in a high noise setting $p = 0.8$: train loss (a), validation accuracy (b) and validation accuracy on the last step in % (c). For each step a mean value across 5 random seeds is plotted, black whiskers in (c) indicate standard deviation. Discover modifications outperform all vanilla optimizers by a large margin, once again suggesting high noise robustness. Adam achieves only 19.8% mean (27.7% max) final accuracy and thus not shown on (c) for clarity.

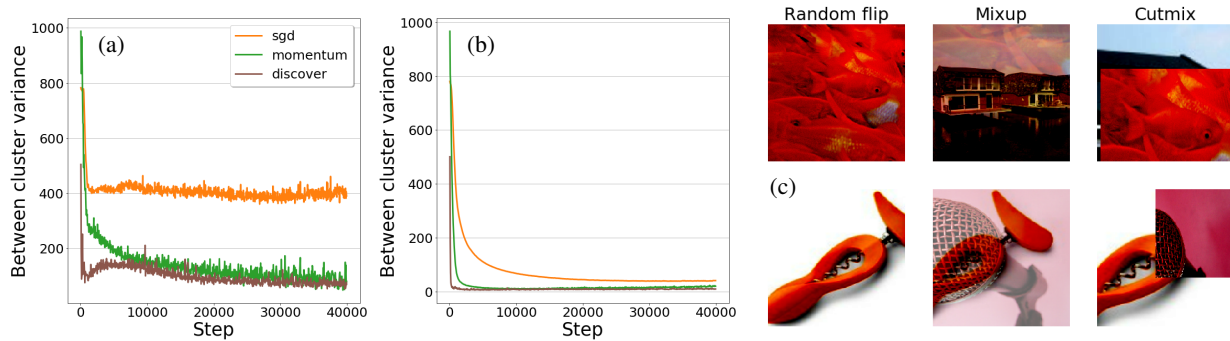


Figure 5. Between-cluster variance estimate (mean per 100 train steps) for CIFAR-10 with clean labels (a) and noisy labels (b) with $p = 0.8$. Example augmentations (c) used as clusters for ImageNet experiments.

References

- TensorFlow Datasets, a collection of ready-to-use datasets. <https://www.tensorflow.org/datasets>.
- Abadi, M., Agarwal, A., Barham, P., Brevdo, E., Chen, Z., Citro, C., Corrado, G. S., Davis, A., Dean, J., Devin, M., Ghemawat, S., Goodfellow, I., Harp, A., Irving, G., Isard, M., Jia, Y., Jozefowicz, R., Kaiser, L., Kudlur, M., Levenberg, J., Mané, D., Monga, R., Moore, S., Murray, D., Olah, C., Schuster, M., Shlens, J., Steiner, B., Sutskever, I., Talwar, K., Tucker, P., Vanhoucke, V., Vasudevan, V., Viégas, F., Vinyals, O., Warden, P., Wattenberg, M., Wicke, M., Yu, Y., and Zheng, X. TensorFlow: Large-scale machine learning on heterogeneous systems, 2015. URL <https://www.tensorflow.org/>. Software available from tensorflow.org.
- Arnold, S., Manzagol, P.-A., Harikandeh, R. B., Mitliagkas, I., and Le Roux, N. Reducing the variance in online optimization by transporting past gradients. In *Advances in Neural Information Processing Systems*, pp. 5392–5403, 2019.
- Bietti, A. and Mairal, J. Stochastic optimization with variance reduction for infinite datasets with finite sum structure. In *Advances in Neural Information Processing Systems*, pp. 1623–1633, 2017.
- Bottou, L., Curtis, F. E., and Nocedal, J. Optimization methods for large-scale machine learning. *Siam Review*, 60(2):223–311, 2018.
- Bradbury, J., Frostig, R., Hawkins, P., Johnson, M. J., Leary, C., Maclaurin, D., and Wanderman-Milne, S. JAX: composable transformations of Python+NumPy programs, 2018. URL <http://github.com/google/jax>.
- Cutkosky, A. and Orabona, F. Momentum-based variance reduction in non-convex sgd. In *Advances in Neural Information Processing Systems*, pp. 15236–15245, 2019.
- Dean, J., Corrado, G., Monga, R., Chen, K., Devin, M., Mao, M., Ranzato, M., Senior, A., Tucker, P., Yang, K., et al. Large scale distributed deep networks. In *Advances in neural information processing systems*, pp. 1223–1231, 2012.
- Defazio, A. and Bottou, L. On the ineffectiveness of variance reduced optimization for deep learning. In *Advances in Neural Information Processing Systems*, pp. 1753–1763, 2019.
- Defazio, A., Bach, F., and Lacoste-Julien, S. Saga: A fast incremental gradient method with support for non-strongly convex composite objectives. In *Advances in neural information processing systems*, pp. 1646–1654, 2014.
- Deng, J., Dong, W., Socher, R., Li, L.-J., Li, K., and Fei-Fei, L. Imagenet: A large-scale hierarchical image database. In *2009 IEEE conference on computer vision and pattern recognition*, pp. 248–255. Ieee, 2009.
- Fishman, G. S. *Monte Carlo: Concepts, Algorithms and Applications*. Springer Verlag, New York, NY, USA, 1996.
- Flax Developers. Flax: A neural network library for jax designed for flexibility, 2020. URL <https://github.com/google-research/flax/tree/prerelease>.
- Goh, G. Why momentum really works. *Distill*, 2(4):e6, 2017.
- Goodfellow, I., Bengio, Y., and Courville, A. *Deep Learning*. MIT Press, 2016. <http://www.deeplearningbook.org>.
- He, K., Zhang, X., Ren, S., and Sun, J. Deep residual learning for image recognition. In *The IEEE Conference on Computer Vision and Pattern Recognition (CVPR)*, June 2016.
- Ioffe, S. and Szegedy, C. Batch normalization: Accelerating deep network training by reducing internal covariate shift. *arXiv preprint arXiv:1502.03167*, 2015.
- Johnson, R. and Zhang, T. Accelerating stochastic gradient descent using predictive variance reduction. In *Advances in neural information processing systems*, pp. 315–323, 2013.
- Jouppi, N. P., Young, C., Patil, N., Patterson, D., Agrawal, G., Bajwa, R., Bates, S., Bhatia, S., Boden, N., Borchers, A., et al. In-datacenter performance analysis of a tensor processing unit. In *Proceedings of the 44th Annual International Symposium on Computer Architecture*, pp. 1–12, 2017.
- Kingma, D. P. and Ba, J. Adam: A method for stochastic optimization. *arXiv preprint arXiv:1412.6980*, 2014.
- Krizhevsky, A., Hinton, G., et al. Learning multiple layers of features from tiny images. 2009.
- Krizhevsky, A., Sutskever, I., and Hinton, G. E. Imagenet classification with deep convolutional neural networks. In *Advances in neural information processing systems*, pp. 1097–1105, 2012.
- Krogh, A. and Hertz, J. A. A simple weight decay can improve generalization. In Moody, J. E., Hanson, S. J., and Lippmann, R. P. (eds.), *Advances in Neural Information Processing Systems 4*, pp. 950–957. Morgan-Kaufmann, 1992. URL <http://papers.nips.cc/paper/>

- 563-a-simple-weight-decay-can-improve-generalization.pdf.
- Li, T., Sahu, A. K., Talwalkar, A., and Smith, V. Federated learning: Challenges, methods, and future directions. *arXiv preprint arXiv:1908.07873*, 2019.
- Loshchilov, I. and Hutter, F. Decoupled weight decay regularization. In *International Conference on Learning Representations*, 2019. URL <https://openreview.net/forum?id=Bkg6RiCqY7>.
- Ma, J. and Yarats, D. Quasi-hyperbolic momentum and adam for deep learning. *arXiv preprint arXiv:1810.06801*, 2018.
- Mairal, J. Optimization with first-order surrogate functions. In *International Conference on Machine Learning*, pp. 783–791, 2013.
- Nemirovski, A., Juditsky, A., Lan, G., and Shapiro, A. Robust stochastic approximation approach to stochastic programming. *SIAM Journal on optimization*, 19(4):1574–1609, 2009.
- Nguyen, L. M., Liu, J., Scheinberg, K., and Takáč, M. Sarah: A novel method for machine learning problems using stochastic recursive gradient. In *Proceedings of the 34th International Conference on Machine Learning-Volume 70*, pp. 2613–2621. JMLR. org, 2017.
- Polyak, B. T. Some methods of speeding up the convergence of iteration methods. *USSR Computational Mathematics and Mathematical Physics*, 4(5):1–17, 1964.
- Qiao, S., Wang, H., Liu, C., Shen, W., and Yuille, A. Weight standardization. *arXiv preprint arXiv:1903.10520*, 2019.
- Robbins, H. E. A stochastic approximation method. *Annals of Mathematical Statistics*, 22:400–407, 2007.
- Roux, N. L., Schmidt, M., and Bach, F. R. A stochastic gradient method with an exponential convergence rate for finite training sets. In *Advances in neural information processing systems*, pp. 2663–2671, 2012.
- Roux, N. L., Babanezhad, R., and Manzagol, P.-A. Online variance-reducing optimization, 2018. URL <https://openreview.net/forum?id=rlqKBtJvG>.
- Russakovsky, O., Deng, J., Su, H., Krause, J., Satheesh, S., Ma, S., Huang, Z., Karpathy, A., Khosla, A., Bernstein, M., Berg, A. C., and Fei-Fei, L. ImageNet Large Scale Visual Recognition Challenge. *International Journal of Computer Vision (IJCV)*, 115(3):211–252, 2015. doi: 10.1007/s11263-015-0816-y.
- Sayed, A. H. Adaptation, learning, and optimization over networks. *Foundations and Trends in Machine Learning*, 7(ARTICLE):311–801, 2014a.
- Sayed, A. H. Adaptive networks. *Proceedings of the IEEE*, 102(4):460–497, 2014b.
- Schmidt, M., Le Roux, N., and Bach, F. Minimizing finite sums with the stochastic average gradient. *Mathematical Programming*, 162(1-2):83–112, 2017.
- Shalev-Shwartz, S. and Ben-David, S. *Understanding machine learning: From theory to algorithms*. Cambridge university press, 2014.
- Shalev-Shwartz, S. and Zhang, T. Stochastic dual coordinate ascent methods for regularized loss minimization. *Journal of Machine Learning Research*, 14(Feb):567–599, 2013.
- Srivastava, N., Hinton, G., Krizhevsky, A., Sutskever, I., and Salakhutdinov, R. Dropout: A simple way to prevent neural networks from overfitting. *J. Mach. Learn. Res.*, 15(1):1929–1958, January 2014a. ISSN 1532-4435.
- Srivastava, N., Hinton, G., Krizhevsky, A., Sutskever, I., and Salakhutdinov, R. Dropout: a simple way to prevent neural networks from overfitting. *The journal of machine learning research*, 15(1):1929–1958, 2014b.
- Sutskever, I., Martens, J., Dahl, G., and Hinton, G. On the importance of initialization and momentum in deep learning. In *International conference on machine learning*, pp. 1139–1147, 2013.
- Szegedy, C., Liu, W., Jia, Y., Sermanet, P., Reed, S., Anguelov, D., Erhan, D., Vanhoucke, V., and Rabinovich, A. Going deeper with convolutions. In *Computer Vision and Pattern Recognition (CVPR)*, 2015. URL <http://arxiv.org/abs/1409.4842>.
- Wu, Y. and He, K. Group normalization. In *The European Conference on Computer Vision (ECCV)*, September 2018.
- Yuan, K., Ying, B., and Sayed, A. H. Cover: A cluster-based variance reduced method for online learning. In *ICASSP 2019-2019 IEEE International Conference on Acoustics, Speech and Signal Processing (ICASSP)*, pp. 3102–3106. IEEE, 2019.
- Yun, S., Han, D., Oh, S. J., Chun, S., Choe, J., and Yoo, Y. Cutmix: Regularization strategy to train strong classifiers with localizable features. In *The IEEE International Conference on Computer Vision (ICCV)*, October 2019a.
- Yun, S., Han, D., Oh, S. J., Chun, S., Choe, J., and Yoo, Y. Cutmix: Regularization strategy to train strong classifiers

with localizable features. In *Proceedings of the IEEE International Conference on Computer Vision*, pp. 6023–6032, 2019b.

Zagoruyko, S. and Komodakis, N. Wide residual networks. *arXiv preprint arXiv:1605.07146*, 2016.

Zhang, H., Cisse, M., Dauphin, Y. N., and Lopez-Paz, D. Mixup: Beyond empirical risk minimization. *arXiv preprint arXiv:1710.09412*, 2017.

Zhang, J. and Mitliagkas, I. Yellowfin and the art of momentum tuning. *arXiv preprint arXiv:1706.03471*, 2017.

7. Appendix A: Experimental details

7.1. Implementation

All models, training and evaluation pipelines are implemented using JAX (Bradbury et al., 2018) and FLAX (Flax Developers, 2020). The data loading and preprocessing is implemented in Tensorflow v2 (Abadi et al., 2015) and TFDS (TFD). The SGD, Momentum and Adam optimizers are taken from FLAX libraries, QHM is implemented following (Ma & Yarats, 2018) and IGT is written in FLAX following an example at https://github.com/google-research/google-research/tree/master/igt_optimizer (Arnold et al., 2019). Discover optimizers are implemented with single-program multiple-data training in mind. Our implementation expects a training data processed during a single training step by a given device core to contain examples from the same cluster. After shuffling the dataset, our input pipeline selects the next $batch_size/num_devices$ examples from the same randomly picked cluster to satisfy this condition. This translates into a single cluster per batch on one-host one-core training (e.g. a workstation with one CPU), but easily scales to more clusters by using multiple cores even within a single-host setting. For examples, the CIFAR experiments use one host machine with 4 Google Cloud TPUv2 (Jouppi et al., 2017) devices, thus having 8 cores in total, so each batch can contain examples from up to 8 different clusters. Discover optimizer averages $g_{\Delta,t} = g(x_t^n, \theta_t) - g_t^{(n)}$ across devices to perform identical \bar{g}_t updates locally on each device and performs local $g_t^{(n)}$ updates in parallel, synchronizing across devices at the end of each training step (see Algorithm 1 for notation). This averaging makes effective α_n value depend on the distributed training setup and to account for it we chose to tune α_n as a direct hyperparameter instead of trying to incorporate the training setup into the formula from Algorithm 1. This implementation is well suited to a good balance of clusters within a single global batch, which is the usual case for a small number of clusters and a randomly shuffled dataset. We have not tested the performance when the cluster distribution in a global batch is significantly skewed.

7.2. Datasets

The datasets used in this work are ImageNet-1000 (Deng et al., 2009; Russakovsky et al., 2015) and CIFAR-10 (Krizhevsky et al., 2009). The datasets were downloaded from <https://www.tensorflow.org/datasets/catalog/imagenet2012> and <https://www.tensorflow.org/datasets/catalog/cifar10> respectively. The detailed information about the size and format of the train and validation splits are available at the corresponding web pages.

7.3. ImageNet (augmentations as clusters)

We trained a ResNet-v1-50 (He et al., 2016) model on the ImageNet (Deng et al., 2009; Russakovsky et al., 2015) dataset for 31200 steps, corresponding to 100 epochs on the unaugmented dataset. We used:

- Cosine learning rate schedule with 5 warmup steps.
- Batch size of 4096.
- Weight decay regularization setting of $\lambda = 0.001$. We used decoupled weight decay inspired by (Loshchilov & Hutter, 2019) and each step update all network parameters by $\Theta_{t+1} = \Theta_t * (1 - \lambda\mu)$ where μ is the learning rate.
- Group normalization with 32 groups (Wu & He, 2018).
- Weight standardization.

The preprocessing consists of Inception-style cropping (Szegedy et al., 2015) with size 224x224, scaling the pixel values to $[-1; 1]$ range and random horizontal flip. In this setting the model achieves 0.76 accuracy with Momentum (Polyak, 1964; Sutskever et al., 2013) optimizer when $\mu = 0.1, \beta = 0.9$. We extend the setting to use Mixup (Zhang et al., 2017) and Cutmix (Yun et al., 2019a) augmentations instead of random flipping, choosing the same mixing ratio for all examples in the single local batch of each distributed training host. We correspondingly assign all examples augmented with random horizontal flip to cluster 0, with Mixup - to cluster 1, Cutmix - to cluster 2. The clusters are used for Discover optimizer.

The hyperparameters are selected from a hyperparameter sweep to obtain the highest mean accuracy at 31200 steps across 5 random seeds. The learning rate μ is chosen from a set of $\{0.03, 0.1, 0.3\}$ for all optimizers. The further hyperparameters are selected from the following sets:

- Discover: $\alpha, \alpha_n \in \{0.001, 0.01, 0.1, 0.9\}$
- Momentum: $\beta \in \{0.85, 0.9, 0.95, 0.99\}$
- QHM: $\beta = 0.999, \gamma = 0.7$ (as reported default for ImageNet in (Ma & Yarats, 2018))
- IGT: $\beta = 0.9, tail_fraction = 90$ (as reported to be selected for ImageNet in (Arnold et al., 2019))
- Adam: $\mu = 0.001, \beta_1 = 0.9, \beta_2 = 0.999$
- Discover-QHM: $\alpha \in \{0.1, 0.6, 0.7, 0.8, 0.9, 0.99\}, \alpha_n \in \{0.01, 0.1, 0.9\}, \beta \in \{0, 1, 0.6, 0.7, 0.8\}$
- Discover-IGT: $\alpha \in \{0.1, 0.6, 0.7, 0.8, 0.9, 0.99\}, \alpha_n \in \{0.01, 0.1, 0.9\}, tail_fraction \in \{18, 45, 50, 60, 90, 180, 360\}$

The exact hyperparameters selected for each optimizer from the hyperparameters sweep are:

- Discover: $\mu = 0.1, \alpha = 0.1, \alpha_n = 0.01$
- Momentum: $\mu = 0.1, \beta = 0.9$
- QHM: $\mu = 0.1$
- IGT: $\mu = 0.1$
- Adam: $\mu = 0.001, \beta_1 = 0.9, \beta_2 = 0.999$
- Discover-QHM: $\mu = 0.1, \alpha = 0.9, \alpha_n = 0.1, \gamma = 0.9$
- Discover-IGT: $\mu = 0.1, \alpha = 0.9, \alpha_n = 0.1, tail_fraction = 180$

The training is setup in the multi-device data-parallel fashion on a pod of 8x8 Google Cloud TPUv3 (Jouppi et al., 2017). There are 16 host machines, each having access to 4 TPUv3 devices. The ImageNet (Deng et al., 2009; Russakovsky et al., 2015) training and validation splits obtained from <https://www.tensorflow.org/datasets/catalog/imagenet2012> are divided into equal parts and each host has access to its own separate part. At most $num_hosts = 16$ examples are excluded this way to ensure the equal division. The training examples inside each batch are arranged such that each device core receives only examples from a single cluster (see Section 7.1). We confirmed that this does not make a practical difference for any other optimizer examined: the loss and accuracy curves look identical and the final accuracy is the same independent of whether this technique is applied or not.

7.4. CIFAR (classes as clusters)

We trained a WideResNet26-10 (Zagoruyko & Komodakis, 2016) model on the CIFAR10 dataset (Krizhevsky et al., 2009) for 400 epochs. We used:

- Cosine learning rate schedule with 5 warmup steps.
- Batch size of 256.
- L2-regularization (Krogh & Hertz, 1992) set to 0.0005.
- Dropout (Srivastava et al., 2014a) rate of 0.3.
- Group normalization (Wu & He, 2018) with 16 groups in the first layer in each block and 32 groups in the rest of the layers.

The preprocessing consists of 4 pixel zero-padding followed by a random crop of size 32x32, scaling the pixels to $[0; 1]$ range and random horizontal flip. We correspondingly assign all examples with the same class to the same cluster (for Discover optimizer).

The hyperparameters are selected from a hyperparameter sweep to obtain the highest mean accuracy at 400 epochs across 5 runs with different random seeds. The learning rate μ is chosen from a set of $\{0.001, 0.01, 0.03, 0.1, 0.175\}$ for all optimizers. The further hyperparameters are selected from the following sets:

- Discover: $\alpha, \alpha_n \in \{0.001, 0.01, 0.015, 0.02, \dots, 0.095, 0.1, 0.15, 0.2, \dots, 0.95, 1.0\}$
- Momentum: $\beta = 0.9$ (as used for WideResNet on CIFAR-10 in (Zagoruyko & Komodakis, 2016))
- QHM: $\beta \in \{0.8, 0.9\}, \gamma \in \{0.1, 0.2, \dots, 0.8, 0.9\}$
- IGT: $\beta = 0.9, tail_fraction = 18$ (as determined to be best for CIFAR-10 in (Arnold et al., 2019))
- Adam: $\beta_1 = 0.9, \beta_2 = 0.999, \epsilon = 1e - 8$ (as a good default settings reported in (Kingma & Ba, 2014))
- Discover-QHM: $\alpha \in \{0.6, 0.7, 0.8, 0.9\}, \alpha_n \in \{0.01, 0.1, 0.9\}, \beta \in \{0.6, 0.7, 0.8, 0.9, 0.99\}$
- Discover-IGT: $\alpha \in \{0.095, 0.1, 0.6, 0.7, 0.8, 0.9, 0.99\}, \alpha_n \in \{0.01, 0.1, 0.9\}, tail_fraction \in \{18, 45, 50, 60, 90, 180, 360\}$

The exact hyperparameters selected for each optimizer from the hyperparameters sweep are:

- SGD: $\mu = 0.01$
- Discover: $\mu = 0.01, \alpha = 0.095, \alpha_n = 0.1$
- Momentum: $\mu = 0.03, \beta = 0.9$
- QHM: $\mu = 0.1, \gamma = 0.9, \beta = 0.9$
- IGT: $\mu = 0.01, \beta = 0.9, tail_fraction = 18$
- Adam: $\mu = 0.001$
- Discover-QHM: $\mu = 0.01, \alpha = 0.9, \alpha_n = 0.1, \beta = 0.9$
- Discover-IGT: $\mu = 0.01, \alpha = 0.095, \alpha_n = 0.1, tail_fraction = 18$

The training setup is the same as for ImageNet experiments (see appendix Section 7.3) but using only one host machine with 4 Google cloud TPUv2 (Jouppi et al., 2017). The CIFAR-10 (Krizhevsky et al., 2009) training and test splits are obtained from <https://www.tensorflow.org/datasets/catalog/cifar10>.

7.5. CIFAR (nosiy labels)

We also run the above-mentioned CIFAR-10 (Krizhevsky et al., 2009) experiments with partially corrupted labels, where the label of each image is flipped to a random different class independently with probability p every time the example is seen during training. E.g. the same example might get different labels in different training epochs. We have tuned the hyperparameters anew in a same way as the clean CIFAR-10 experiment above Section 7.4 each value of $p \in \{0.2, 0.8\}$. The results for the low-noise setting ($p = 0.2$) and high-noise setting ($p = 0.8$) are reported in Figure 6 and Figure 4 respectively.

The exact hyperparameters selected for $p = 0.2$ setting are:

- SGD: $\mu = 0.175$

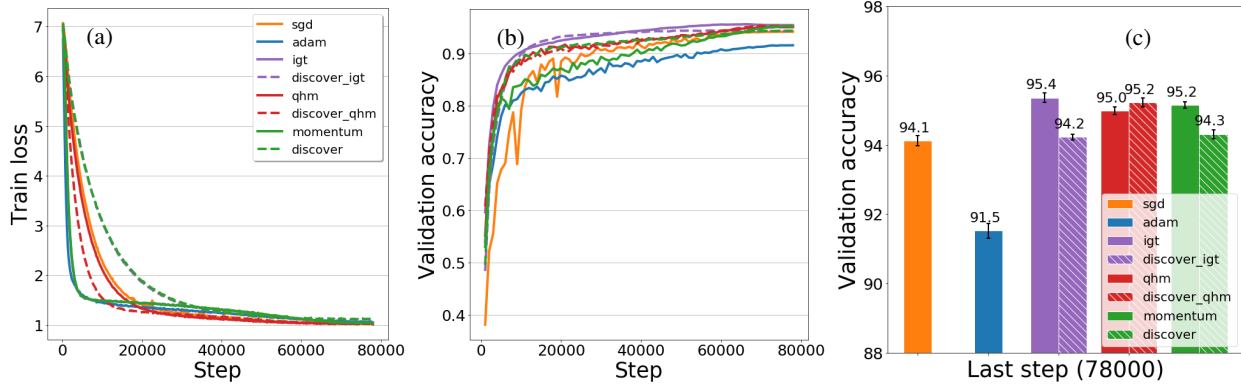


Figure 6. Results of training WideResNet26-10 model on CIFAR-10 dataset (classes as clusters) in a low noise setting $p = 0.2$: train loss (a), validation accuracy (b) and validation accuracy on the last step in % (c). For each step a mean value across 5 random seeds is plotted, black whiskers in (c) indicate standard deviation.

- Discover: $\mu = 0.01, \alpha = 0.095, \alpha_n = 0.1$
- Momentum: $\mu = 0.1, \beta = 0.9$
- QHM: $\mu = 0.175, \gamma = 0.9, \beta = 0.9$
- IGT: $\mu = 0.1, \beta = 0.9, tail_fraction = 18$
- Adam: $\mu = 0.001$
- Discover-QHM: $\mu = 0.1, \alpha = 0.9, \alpha_n = 0.1, \gamma = 0.7$
- Discover-IGT: $\mu = 0.1, \alpha = 0.095, \alpha_n = 0.1, tail_fraction = 18$

The exact hyperparameters selected for $p = 0.8$ setting are:

- SGD: $\mu = 0.1$
- Discover: $\mu = 0.01, \alpha = 0.095, \alpha_n = 0.1$
- Momentum: $\mu = 0.01, \beta = 0.9$
- QHM: $\mu = 0.1, \gamma = 0.6, \beta = 0.9$
- IGT: $\mu = 0.01, \beta = 0.9, tail_fraction = 18$
- Adam: $\mu = 0.001$
- Discover-QHM: $\mu = 0.1, \alpha = 0.6, \alpha_n = 0.1, \gamma = 0.6$
- Discover-IGT: $\mu = 0.1, \alpha = 0.095, \alpha_n = 0.1, tail_fraction = 18$

7.6. ImageNet (noisy labels)

We also run the above-mentioned ImageNet (Deng et al., 2009; Russakovsky et al., 2015) experiments with partially corrupted labels, where the label of each image is flipped to a random different class independently with probability $p = 0.8$ every time the example is seen during training. E.g. the same example might get different labels in different training epochs. We used the same hyperparameters as selected for the clean ImageNet experiment, except the learning rate which was selected again for each optimizer value of p as described in Section 7.3. The best values were exactly the values chosen in Section 7.3.

7.7. CIFAR (augmentations as clusters)

We also run the above-mentioned CIFAR-10 experiments when using Mixup, Cutmix and left-right flipping augmented examples as clusters to mirror the setting used for ImageNet experiments above. We did not tune any hyperparameters anew, instead for both clean and noisy labels setting we have used the same hyperparameters as for the experiments above (when classes were used as clusters). When using clean labels the results for Discover modifications shown on Figure 7 were very similar to those of vanilla optimizers as expected. When using noisy labels (with $p = 0.8$) Discover modifications performed significantly worse than vanilla optimizers as shown on Figure 8. These results highlight the importance of the careful clustering structure choice and suggest that Discover hyperparameters chosen for one clustering structure does not necessarily transfer to a different clustering choice in case of noisy labels.

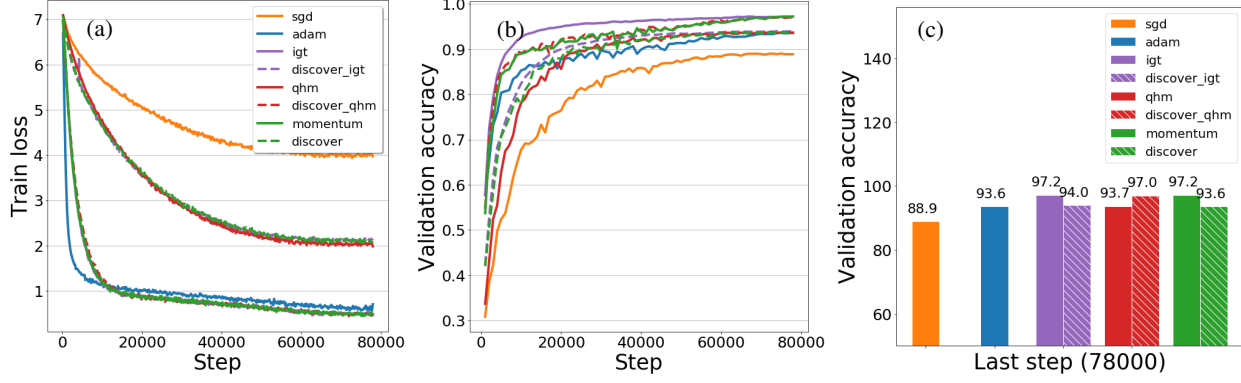


Figure 7. Results of training WideResNet26-10 model on CIFAR-10 dataset (Mixup, Cutmix and left-right flipping augmented examples as clusters) in a clean labels setting: train loss (a), validation accuracy (b) and validation accuracy on the last step in % (c).

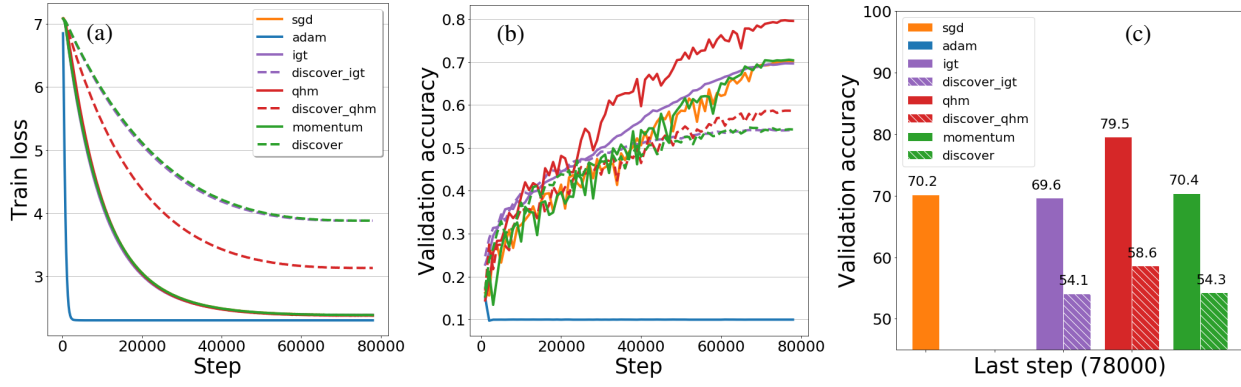


Figure 8. Results of training WideResNet26-10 model on CIFAR-10 dataset (Mixup, Cutmix and left-right flipping augmented examples as clusters) in a high noise ($p = 0.8$) setting: train loss (a), validation accuracy (b) and validation accuracy on the last step in % (c).

8. Variance due to label noise

Suppose that we optimize the loss $\ell(f_\theta(x)) := \ell(\theta; x, f_\theta(x))$ with gradient equal to $g(x, \theta)$. Let denote by $\tilde{g}(x, \theta)$ the gradient of the loss $\ell(F_\theta(x))$ where $F(x)$ is the true labeling function. On an instance x , we can write it as: $\ell(f_\theta(x)) = a + b$, with $a = \ell(F_\theta(x))$ and $b = \ell(f_\theta(x)) - \ell(F_\theta(x))$.

$$\begin{aligned} \mathbb{E}\|g(x, \theta)\|^2 &= \mathbb{E}\|\tilde{g}(x, \theta) + g(x, \theta) - \tilde{g}(x, \theta)\|^2 \\ &\leq 2\mathbb{E}\|\tilde{g}(x, \theta)\|^2 + 2\mathbb{E}\|g(x, \theta) - \tilde{g}(x, \theta)\|^2 \end{aligned}$$

The first term is the traditional variance of the gradient noise, and the second term is due to the label noise the larger the noise the larger it is.

9. Appendix B: Proofs

Proof 1 Before proving, we denote $\mathbb{E}[\cdot] = \mathbb{E}_{n,t}[\cdot | x_t^n]$ and $\mathbb{E}_t = \mathbb{E}[\cdot | F_t]$ where the superscript n indicate the cluster index x arises from.

In this part we want to give a proof of [Lemma 1](#). We want to show that the first and second order moments of the gradient noise $s_{t+1}(\theta_t)$ satisfy :

$$\mathbb{E}\left(s_{t+1}(\theta_t) | F_t\right) = 0 \quad (8)$$

$$\mathbb{E}\left(\|s_{t+1}(\theta_t)\|^2 | F_t\right) \leq \beta^2 \|\tilde{\theta}_t\|^2 + \sigma^2 \quad (9)$$

where $\tilde{\theta}_t = \theta_t - \theta^*$, $\beta^2 = 2\delta^2$ and :

$$\begin{aligned} \sigma^2 &= 2\mathbb{E}\left(\|g(x_t^n, \theta^*)\|^2\right) \\ &= 2\sum_{n=1}^N p_n \mathbb{E}_t\left(\|g(x_t^n, \theta^*)\|^2\right) \end{aligned}$$

where σ^2 is referred to as the magnitude of gradient noise. In case all the clusters have the same probability that is

$p_1 = p_2, \dots, p_N = \frac{1}{N}$, we have that:

$$\begin{aligned}\sigma^2 &= 2\mathbb{E}\left(\|g(x_t^n, \theta^*)\|^2\right) \\ &= 2\sum_{n=1}^N p_n \mathbb{E}_t\left(\|g(x_t^n, \theta^*)\|^2\right) \\ &= 2\mathbb{E}_t\left(\|g(x_t, \theta^*)\|^2\right)\end{aligned}$$

which correspond to the magnitude of gradient noise without considering the clustering structure.

we recall that the gradient noise for SGD is given by :

$$s_{t+1}(\theta_t) = g(x_t^n, \theta_t) - g(\theta_t).$$

$$\begin{aligned}\mathbb{E}\left(s_{t+1}(\theta_t)|F_t\right) &= \mathbb{E}_{n,t}\left(g(x_t^n, \theta_t)|F_t\right) - g(\theta_t) \\ &= \sum_{n=1}^N p_n g_n(\theta_t) - g(\theta_t) \\ &= 0\end{aligned}$$

Where we use the fact that :

$$\begin{aligned}g_n(\theta_t) &= \mathbb{E}_t\left(g(x_t^n, \theta_t)|F_t\right) \\ g(\theta_t) &= \mathbb{E}_n(g_n(\theta_t))\end{aligned}$$

Using the following Jensen's inequality :

$$\begin{aligned}\mathbb{E}(\|a + b\|^2) &= 4\mathbb{E}(\|\frac{1}{2}a + \frac{1}{2}b\|^2) \\ &\leq 2\mathbb{E}(\|a\|^2) + 2\mathbb{E}(\|b\|^2)\end{aligned}$$

It holds that :

$$\begin{aligned}\mathbb{E}\left(\|s_{t+1}(\theta_t)\|^2|F_t\right) &= \mathbb{E}\left(\|g(x_t^n, \theta_t) - g(\theta_t)\|^2|F_t\right) \\ &\leq 2\mathbb{E}\left(\|g(x_t^n, \theta_t) - g(\theta_t) - g(x_t^n, \theta^*)\|^2|F_t\right) \\ &+ 2\mathbb{E}\left(\|g(x_t^n, \theta^*)\|^2|F_t\right)\end{aligned}$$

Using the fact that for any random variable x ,

$$\mathbb{E}\|x - E[x]\|^2 = \mathbb{E}\|x\|^2 - \|\mathbb{E}[x]\|^2 \leq \mathbb{E}\|x\|^2$$

and $g(\theta^*) = 0$, we have :

$$\begin{aligned}\mathbb{E}\left(\|g(x_t^n, \theta_t) - g(\theta_t) - g(x_t^n, \theta^*)\|^2|F_t\right) &\leq \mathbb{E}\left(\|g(x_t^n, \theta_t) - g(x_t^n, \theta^*)\|^2|F_t\right) \\ &\leq \delta^2 \|\tilde{\theta}_t\|^2\end{aligned}$$

We recall that the gradient noise *within* the cluster n is given by:

$$s_{t+1}^n(\theta_t) = g(x_t^n, \theta_t) - g_n(\theta_t)$$

Assuming the gradient noise *within* the cluster n is following assumptions similar to the result in [Lemma 1](#) meaning that it is unbiased and its variance is bounded : $\mathbb{E}(\|s_{t+1}^n(\theta_t)\|^2|F_t) \leq \gamma_n^2 \|\tilde{\theta}_t\|^2 + \sigma_n^2$, where $\tilde{\theta}_t = \theta^* - \theta_t$, and $\gamma_n, \sigma_n > 0$, where σ_n^2 is referred to as the magnitude of gradient noise in cluster n . we want to prove [Lemma 2](#) :

$$\mathbb{E}(\|s_{t+1}(\theta^*)\|^2|F_t) \leq \underbrace{\sum_{n=1}^N p_n \sigma_n^2}_{\text{in-cluster variance}} + \underbrace{\sum_{n=1}^N p_n \|g_n(\theta^*)\|^2}_{\text{between-cluster variance}} \quad (10)$$

Proof 2

From (Yuan et al., 2019) it holds that :

$$\begin{aligned}
\mathbb{E}(\|s_{t+1}(\theta^*)\|^2|F_t) &= \mathbb{E}(\|g(x_t^n, \theta^*)\|^2|F_t) & \mathbb{E}\left(\|u_{t+1}^n(\theta_t)\|^2|F_t\right) &\leq C_1\|\tilde{\theta}_t\|^2 + C_2 + \\
&= \mathbb{E}(\|g(x_t^n, \theta_t) - g_n(\theta^*) + g_n(\theta^*)\|^2|F_t) & \\
&= \mathbb{E}(\|s_{t+1}^n(\theta^*) + g_n(\theta^*)\|^2|F_t) & \\
&= \mathbb{E}(\|s_{t+1}^n(\theta^*)\|^2|F_t) + \mathbb{E}(\|g_n(\theta^*)\|^2|F_t) & 2 \sum_{n=1}^N p_n \|g_t^{(n)} - g_n(\theta^*)\|^2 \\
&\leq \sum_{n=1}^N p_n (\gamma_n^2 \|0\|^2 + \sigma_n^2) + &
\end{aligned}$$

Now we can give properties of DISCOVER gradient noise by proving Lemma 3:

$$\begin{aligned}
&\sum_{n=1}^N p_n \|g_n(\theta^*)\|^2 \\
\mathbb{E}(\|s_{t+1}(\theta^*)\|^2|F_t) &\leq \sum_{n=1}^N p_n \sigma_n^2 + \sum_{n=1}^N p_n \|g_n(\theta^*)\|^2
\end{aligned}$$

where the expectation is also taken over the different clusters with probabilities p_n .

9.1. Proof of Lemma 3

Under the same assumptions as in Section 3, for a batch of size $|\mathcal{B}_t|$ the gradient is unbiased $E[u_{t+1}(\theta_t)|F_t] = 0$. Denoting $\tilde{\theta}_t := \theta^* - \theta_t$, $C_1 = 4\delta^2$, $C_2 = \sum_{n=1}^N p_n \sigma_n^2$ and $\sigma_n^2 = 2 \cdot \mathbb{E}(\|g(x_t^n, \theta^*)\|^2)$.

The gradient noise of DISCOVER is given by the following:

$$\begin{aligned}
u_{t+1}(\theta_t) &= \frac{1}{|\mathcal{B}_t|} \cdot \sum_{x_t^n \in \mathcal{B}_t} \left(g(x_t^n, \theta_t) - g_t^{(n)} + \bar{g}_t - g(\theta_t) \right) \\
&= \frac{1}{|\mathcal{B}_t|} \sum_{x_t^n \in \mathcal{B}_t} u_{t+1}^n(\theta_t)
\end{aligned}$$

where

$$u_{t+1}^n(\theta_t) = g(x_t^n, \theta_t) - g_t^{(n)} + \bar{g}_t - g(\theta_t)$$

To this end, we introduce the filtration $F_t = \{\theta_{i < t+1}\}$.

Since $\theta_t \in F_t$ and the cluster n is selected with probability p_n , it holds that

$$\begin{aligned}
E[u_{t+1}^n(\theta_t)|F_t] &= \mathbb{E}\left(g(x_t^n, \theta_t) - g_t^{(n)} + \bar{g}_t - g(\theta_t)|F_t\right) \\
&= \mathbb{E}\left(g(x_t^n, \theta_t) - g(\theta_t)|F_t\right) + \mathbb{E}\left(\bar{g}_t - g_t^{(n)}|F_t\right) \\
&= \mathbb{E}\left(s_{t+1}(\theta_t)|F_t\right) + \bar{g}_t - \sum_{n=1}^N p_n g_t^{(n)} \\
&= 0
\end{aligned}$$

Because $s_{t+1}(\theta_t) = g(x_t^n, \theta_t) - g(\theta_t)$ and $\bar{g}_t = \sum_{n=1}^N p_n g_t^{(n)}$.

$$\begin{aligned}
 E[u_{t+1}(\theta_t)|F_t] &= \mathbb{E}\left(\frac{1}{|\mathcal{B}_t|} \sum_{x_t^n \in \mathcal{B}_t} u_{t+1}^n(\theta_t)|F_t\right) \\
 &= \frac{1}{|\mathcal{B}_t|} \sum_{x_t^n \in \mathcal{B}_t} \mathbb{E}\left(u_{t+1}^n(\theta_t)|F_t\right) \\
 &= 0
 \end{aligned}$$

$$\begin{aligned}
 \mathbb{E}\left(\|u_{t+1}(\theta_t)\|^2 \middle| F_t\right) &= \mathbb{E}\left(\left\|\frac{1}{|\mathcal{B}_t|} \sum_{x_t^n \in \mathcal{B}_t} u_{t+1}^n(\theta_t)\right\|^2 \middle| F_t\right) \\
 &= \frac{1}{|\mathcal{B}_t|^2} \cdot \mathbb{E}\left(\left\|\sum_{x_t^n \in \mathcal{B}_t} u_{t+1}^n(\theta_t)\right\|^2 \middle| F_t\right) \\
 &= \frac{1}{|\mathcal{B}_t|^2} \cdot \mathbb{E}\left(\sum_{x_t^n \in \mathcal{B}_t} \left\|u_{t+1}^n(\theta_t)\right\|^2 \middle| F_t\right) + \\
 &\frac{1}{|\mathcal{B}_t|^2} \cdot \mathbb{E}\left(\sum_{x_t^n \in \mathcal{B}_t} \sum_{x_t^m \neq x_t^n} \left(u_{t+1}^n(\theta_t)\right)^T \left(u_{t+1}^m(\theta_t)\right) \middle| F_t\right) \\
 &= \frac{1}{|\mathcal{B}_t|^2} \cdot \mathbb{E}\left(\sum_{x_t^n \in \mathcal{B}_t} \left\|u_{t+1}^n(\theta_t)\right\|^2 \middle| F_t\right) \\
 &= \frac{1}{|\mathcal{B}_t|^2} \cdot \sum_{x_t^n \in \mathcal{B}_t} \mathbb{E}\left(\left\|u_{t+1}^n(\theta_t)\right\|^2 \middle| F_t\right)
 \end{aligned}$$

In the above proof we use the fact that the gradient noise are independent from one cluster to another meaning that for $n \neq m$:

$$\mathbb{E}\left(u_{t+1}^n(\theta_t)u_{t+1}^m(\theta_t)|F_t\right) = \mathbb{E}\left(u_{t+1}^n(\theta_t)|F_t\right)\mathbb{E}\left(u_{t+1}^m(\theta_t)|F_t\right) = 0$$

So we have :

$$\begin{aligned}
 \mathbb{E}\left(\|u_{t+1}(\theta_t)\|^2 \middle| F_t\right) &= \frac{1}{|\mathcal{B}_t|^2} \cdot \sum_{x_t^n \in \mathcal{B}_t} \mathbb{E}\left(\|u_{t+1}^n(\theta_t)\|^2 \middle| F_t\right) \\
 &\leq \frac{1}{|\mathcal{B}_t|^2} \cdot \sum_{x_t^n \in \mathcal{B}_t} \left(C_1 \|\tilde{\theta}_t\|^2 + C_2 + 2 \sum_{n=1}^N p_n \|g_t^{(n)} - g_n(\theta^*)\|^2\right) \\
 &\leq \frac{1}{|\mathcal{B}_t|} \cdot C_1 \|\tilde{\theta}_t\|^2 + \frac{1}{|\mathcal{B}_t|} \cdot C_2 + \frac{2}{|\mathcal{B}_t|} \cdot \sum_{n=1}^N p_n \|g_t^{(n)} - g_n(\theta^*)\|^2
 \end{aligned}$$

Lemma 4 Under the same assumptions as in Section 3, for a batch of size $|\mathcal{B}_t|$, defining G_t to be :

$$G_t = \sum_{n=1}^N p_n \mathbb{E} \left(\|g_t^{(n)} - g_n(\theta^*)\|^2 \right)$$

The two inequalities hold:

$$\mathbb{E} \left(\|\tilde{\theta}_{t+1}\|^2 \right) \leq \left(1 - 2\mu\nu + \mu^2(\delta^2 + \frac{C_1}{|\mathcal{B}_t|}) \right) \mathbb{E}(\|\tilde{\theta}_t\|^2) + \frac{\mu^2}{|\mathcal{B}_t|} C_2 + \frac{2\mu^2}{|\mathcal{B}_t|} \cdot G_t$$

$$G_{t+1} \leq (1 - \alpha) \cdot G_t + 3\alpha\delta^2 \cdot \mathbb{E}(\|\tilde{\theta}_t\|^2) + \alpha C_2 \quad (11)$$

9.2. Proof of Lemma 4

Before proving Lemma 4, we are going to use the following lemma from (Sayed, 2014a):

Lemma 5 (Mean-value theorem: Real arguments)

Consider a real-valued and twice-differentiable function $g(z) \in \mathbb{R}$, where $z \in \mathbb{R}^M$ is real-valued. Then for any M -dimensional vectors z_0 and Δz , the following increment equalities hold:

$$g(z_0 + \Delta z) - g(z_0) = \left(\int_0^1 \nabla_z g(z_0 + t\Delta z) dt \right) \Delta z \quad (12)$$

$$\nabla_z g(z_0 + \Delta z) - \nabla_z g(z_0) = (\Delta z)^T \left(\int_0^1 \nabla_z^2 g(z_0 + r\Delta z) dr \right) \quad (13)$$

From Lemma 5, denoting $\tilde{\theta}_t := \theta^* - \theta_t$, $g(\theta) = \nabla \ell(f(\theta, x^n))$, we have:

$$\begin{aligned} g(\theta_t) &= - \left(\int_0^1 \nabla_{\theta} g(\theta^* - t\tilde{\theta}_t) dt \right) \tilde{\theta}_t \\ &:= -H_t \tilde{\theta}_t \end{aligned}$$

where we are introducing the symmetric time-variant matrix which is defined in terms of the Hessian of the cost function.

$$H_t := \int_0^1 \nabla_{\theta} g(\theta^* - t\tilde{\theta}_t) dt$$

Considering DISCOVER recursion in Algorithm 1 under the same assumptions as in Section 3, for a batch of size

$|\mathcal{B}_t|$ and using the particular result of Lemma 5 we have:

$$\begin{aligned} \theta_{t+1} &= \theta_t - \frac{\mu}{|\mathcal{B}_t|} \cdot \sum_{x_t^n \in \mathcal{B}_t} \left(g(x_t^n, \theta_t) - g_t^{(n)} + \bar{g}_t \right) \\ -\theta_{t+1} &= -\theta_t + \frac{\mu}{|\mathcal{B}_t|} \cdot \sum_{x_t^n \in \mathcal{B}_t} \left(g(x_t^n, \theta_t) - g_t^{(n)} + \bar{g}_t \right) \\ &= -\theta_t + \frac{\mu}{|\mathcal{B}_t|} \cdot \sum_{x_t^n \in \mathcal{B}_t} \left(g(x_t^n, \theta_t) - g_t^{(n)} + \bar{g}_t - g(\theta_t) \right) \\ &\quad + g(\theta_t) \\ &= -\theta_t + \frac{\mu}{|\mathcal{B}_t|} \cdot \sum_{x_t^n \in \mathcal{B}_t} \left(g(x_t^n, \theta_t) - g_t^{(n)} + \bar{g}_t - g(\theta_t) \right) \\ &\quad + \mu \cdot g(\theta_t) \\ &= -\theta_t + \mu \cdot g(\theta_t) + \mu \cdot u_{t+1}(\theta_t) \\ \tilde{\theta}_{t+1} &= \tilde{\theta}_t - \mu \cdot H_t \cdot \tilde{\theta}_t + \mu \cdot u_{t+1}(\theta_t) \\ \tilde{\theta}_{t+1} &= (I - \mu \cdot H_t) \tilde{\theta}_t + \mu \cdot u_{t+1}(\theta_t) \end{aligned}$$

Since :

$$0 < \nu I_d < \nabla g(\theta) < \delta I_d$$

where d is the dimension of θ and $\nabla g(\theta)$ is the Hessian Matrix, we can derive:

$$(1 - \mu\delta)I_d < I_d - \mu H_t < (1 - \mu\nu)I_d$$

for all t . Using the fact that $I_d - \mu H_t$ is a symmetric matrix, we have that its 2-induced norm is equal to its spectral radius so that:

$$\begin{aligned} \|I - \mu \cdot H_t\|^2 &= \left(\rho(I - \mu \cdot H_t) \right)^2 \\ &\leq \max \left\{ (1 - \mu\delta)^2, (1 - \mu\nu)^2 \right\} \\ &= \max \left\{ 1 - 2\mu\delta + \mu^2\delta^2, 1 - 2\mu\nu + \mu^2\nu^2 \right\} \\ \|I - \mu \cdot H_t\|^2 &\leq 1 - 2\mu\delta + \mu^2\delta^2 \end{aligned}$$

We got the last inequality because $\nu \leq \delta$

Using the previous result, we have :

$$\begin{aligned}
 \|\tilde{\theta}_{t+1}\|^2 &\leq \|I - \mu \cdot H_t\|^2 \cdot \|\tilde{\theta}_t\|^2 + \mu^2 \cdot \|u_{t+1}(\theta_t)\|^2 \\
 \mathbb{E}\left(\|\tilde{\theta}_{t+1}\|^2 | F_t\right) &\leq \|I - \mu \cdot H_t\|^2 \cdot \mathbb{E}(\|\tilde{\theta}_t\|^2 | F_t) + \mu^2 \mathbb{E}\left(\|u_{t+1}(\theta_t)\|^2 | F_t\right) \\
 &\leq (1 - 2\mu\nu + \mu^2\delta^2) \mathbb{E}(\|\tilde{\theta}_t\|^2 | F_t) + \mu^2 \left(\frac{1}{|\mathcal{B}_t|} C_1 \mathbb{E}(\|\tilde{\theta}_t\|^2 | F_t) + \frac{1}{|\mathcal{B}_t|} C_2 + \frac{2}{|\mathcal{B}_t|} \sum_{n=1}^N p_n \|g_t^{(n)} - g_n(\theta^*)\|^2 \right) \\
 &\leq \left(1 - 2\mu\nu + \mu^2(\delta^2 + \frac{C_1}{|\mathcal{B}_t|}) \right) \mathbb{E}(\|\tilde{\theta}_t\|^2 | F_t) + \frac{\mu^2}{|\mathcal{B}_t|} C_2 + \frac{2\mu^2}{|\mathcal{B}_t|} \cdot \sum_{n=1}^N p_n \|g_t^{(n)} - g_n(\theta^*)\|^2
 \end{aligned}$$

Then taking the expectation on both side give us:

$$\mathbb{E}\left(\|\tilde{\theta}_{t+1}\|^2\right) \leq \left(1 - 2\mu\nu + \mu^2(\delta^2 + \frac{C_1}{|\mathcal{B}_t|}) \right) \mathbb{E}(\|\tilde{\theta}_t\|^2) + \frac{\mu^2}{|\mathcal{B}_t|} C_2 + \frac{2\mu^2}{|\mathcal{B}_t|} \cdot \sum_{n=1}^N p_n \mathbb{E}(\|g_t^{(n)} - g_n(\theta^*)\|^2)$$

which conclude the proof. The second equation of [Lemma 4](#) is obtained from Lemma 2 of ([Yuan et al., 2019](#)).

9.3. Proof of Theorem 1

From Lemma 4, we have :

$$\begin{aligned}
\mathbb{E}(\|\tilde{\theta}_{t+1}\|^2) + \gamma G_{t+1} &\leq \left(1 - 2\mu\nu + \mu^2(\delta^2 + \frac{C_1}{|\mathcal{B}_t|})\right) \mathbb{E}(\|\tilde{\theta}_t\|^2) + \frac{\mu^2}{|\mathcal{B}_t|} C_2 + \frac{2\mu^2}{|\mathcal{B}_t|} \cdot G_t + \\
\gamma \left((1 - \alpha) \cdot G_t + 3\alpha\delta^2 \cdot \mathbb{E}(\|\tilde{\theta}_t\|^2) + \alpha C_2 \right) \\
&= \left[1 - 2\mu\nu + \mu^2(\delta^2 + \frac{C_1}{|\mathcal{B}_t|}) + 3\alpha\gamma\delta^2 \right] \mathbb{E}(\|\tilde{\theta}_t\|^2) + \left(\frac{\mu^2}{|\mathcal{B}_t|} + \alpha\gamma \right) C_2 + \\
\left(\frac{2\mu^2}{|\mathcal{B}_t|} + \gamma(1 - \alpha) \right) \cdot G_t \\
&\leq \left[1 - 2\mu\nu + K \right] \mathbb{E}(\|\tilde{\theta}_t\|^2) + \left(\frac{\mu^2}{|\mathcal{B}_t|} + \alpha\gamma \right) C_2 + \left(\frac{2\mu^2}{|\mathcal{B}_t|} + \gamma(1 - \alpha) \right) \cdot G_t \\
&\leq \left[1 - 2\mu\nu + K \right] \left(\mathbb{E}(\|\tilde{\theta}_t\|^2) + \frac{\left(\frac{2\mu^2}{|\mathcal{B}_t|} + \gamma(1 - \alpha) \right)}{1 - 2\mu\nu + K} \cdot G_t \right) + \\
\left(\frac{\mu^2}{|\mathcal{B}_t|} + \alpha\gamma \right) C_2 \\
&\leq \left[1 - 2\mu\nu + K \right] \left(\mathbb{E}(\|\tilde{\theta}_t\|^2) + \frac{\left(\frac{2\mu^2}{|\mathcal{B}_t|} + \gamma(1 - \alpha) \right)}{1 - 2\mu\nu} \cdot G_t \right) + \\
\left(\frac{\mu^2}{|\mathcal{B}_t|} + \alpha\gamma \right) C_2 \\
&\leq (1 - \mu\nu) \left(\mathbb{E}(\|\tilde{\theta}_t\|^2) + \frac{\left(\frac{2\mu^2}{|\mathcal{B}_t|} + \gamma(1 - \alpha) \right)}{1 - 2\mu\nu} \cdot G_t \right) + \left(\frac{\mu^2}{|\mathcal{B}_t|} + \alpha\gamma \right) C_2 \\
&\leq (1 - \mu\nu) \left(\mathbb{E}(\|\tilde{\theta}_t\|^2) + \gamma \cdot G_t \right) + \left(\frac{\mu^2}{|\mathcal{B}_t|} + \alpha\gamma \right) C_2 \\
\mathbb{E}(\|\tilde{\theta}_{t+1}\|^2) + \gamma G_{t+1} &\leq (1 - \mu\nu) \left(\mathbb{E}(\|\tilde{\theta}_t\|^2) + \gamma \cdot G_t \right) + \frac{4\mu^2}{|\mathcal{B}_t|} \cdot C_2
\end{aligned}$$

Since μ satisfies $\mu \leq \frac{\alpha}{6\nu}$

$$\begin{aligned}\alpha - 6\mu\nu &\geq 0 \\ 3\alpha - 6\mu\nu &\geq 2\alpha \\ \frac{3}{\alpha} &\geq \frac{2}{\alpha - 2\mu\nu} \\ \gamma = \frac{3\mu^2}{\alpha|\mathcal{B}_t|} &\geq \frac{2\mu^2}{|\mathcal{B}_t|(\alpha - 2\mu\nu)}\end{aligned}$$

$$\gamma \geq \frac{2\mu^2}{|\mathcal{B}_t|(\alpha - 2\mu\nu)} \Leftrightarrow \gamma \geq \frac{\left(\frac{2\mu^2}{|\mathcal{B}_t|} + \gamma(1 - \alpha)\right)}{1 - 2\mu\nu} \quad (14)$$

Because

$$\gamma = \frac{\left(\frac{2\mu^2}{|\mathcal{B}_t|} + \gamma(1 - \alpha)\right)}{1 - 2\mu\nu} \Leftrightarrow \gamma = \frac{2\mu^2}{|\mathcal{B}_t|(\alpha - 2\mu\nu)} \quad (15)$$

Also since μ satisfies $\mu \leq \frac{\nu|\mathcal{B}_t|}{3\delta^2(|\mathcal{B}_t|+5)}$

It implies that :

$$\begin{aligned}\mu\left(1 + \frac{5}{|\mathcal{B}_t|}\right) &\leq \frac{\nu}{3\delta^2} \\ \mu^2\left(1 + \frac{5}{|\mathcal{B}_t|}\right) &\leq \frac{\mu\nu}{3\delta^2} \\ \mu^2 + \frac{2\mu^2}{|\mathcal{B}_t|} + \frac{3\mu^2}{|\mathcal{B}_t|} &\leq \frac{\mu\nu}{3\delta^2} \\ \mu^2 + \frac{2\mu^2}{|\mathcal{B}_t|} + \alpha\gamma &\leq \frac{\mu\nu}{3\delta^2} \\ 3\delta^2\left(\mu^2 + \frac{2\mu^2}{|\mathcal{B}_t|} + \alpha\gamma\right) &\leq \mu\nu \\ 1 - 2\mu\nu + 3\delta^2\left(\mu^2 + \frac{2\mu^2}{|\mathcal{B}_t|} + \alpha\gamma\right) &\leq 1 - 2\mu\nu + \mu\nu \\ 1 - 2\mu\nu + K &\leq 1 - \mu\nu\end{aligned}$$

So in conclusion :

$$1 - 2\mu\nu + K \leq 1 - \mu\nu \quad (16)$$

In summary we have :

Iterating recursion above we get :

$$\begin{aligned}
 \mathbb{E}(\|\tilde{\theta}_{t+1}\|^2) &\leq \mathbb{E}(\|\tilde{\theta}_{t+1}\|^2) + \gamma G_{t+1} \leq (1 - \mu\nu) \cdot \left(\mathbb{E}(\|\tilde{\theta}_t\|^2) + \gamma G_t \right) + \frac{4\mu^2}{|\mathcal{B}_t|} C_2 \\
 &\leq (1 - \mu\nu)^{t+1} \cdot \left(\mathbb{E}(\|\tilde{\theta}_0\|^2) + \gamma G_0 \right) + \frac{4\mu^2}{|\mathcal{B}_t|} C_2 \sum_{k=0}^t (1 - \mu\nu)^k \\
 &\leq (1 - \mu\nu)^{t+1} \cdot \left(\mathbb{E}(\|\tilde{\theta}_0\|^2) + \gamma G_0 \right) + \frac{1}{1 - (1 - \mu\nu)} \frac{4\mu^2}{|\mathcal{B}_t|} C_2 \\
 &\leq (1 - \mu\nu)^{t+1} \cdot \left(\mathbb{E}(\|\tilde{\theta}_0\|^2) + \gamma G_0 \right) + \frac{4\mu}{\nu|\mathcal{B}_t|} C_2
 \end{aligned}$$

That implies :

$$\mathbb{E}(\|\tilde{\theta}_{t+1}\|^2) \leq (1 - \mu\nu)^{t+1} \cdot \left(\mathbb{E}(\|\tilde{\theta}_0\|^2) + \gamma G_0 \right) + \frac{4\mu}{\nu|\mathcal{B}_t|} C_2 \tag{17}$$

So that :

$$\limsup_{t \rightarrow +\infty} \mathbb{E}(\|\theta^* - \theta_{t+1}\|^2) = O\left(\frac{\mu}{|\mathcal{B}_t|} C_2\right) = O(\mu \cdot \sigma_{in}^2 / |\mathcal{B}_t|) \tag{18}$$